ACS MATERIALS LETTERS

www.acsmaterialsletters.org

Near-Infrared Light-Responsive Nanosystem with Prolonged Circulation and Enhanced Penetration for Increased Photothermal and Photodynamic Therapy

Fangli Gao,[▽] Liting Jiang,[▽] Jie Zhang, Yi Chang, Weihua Gao, Lina Ding, Guanglei Ma, Xiaoming Ma,* and Yuming Guo*

Cite This: *ACS Materials Lett.* 2023, 5, 1−10

Read Online

ACCESS | Metrics & More | Article Recommendations | Supporting Information

ABSTRACT: It is still a challenge to optimize the tumor therapeutic efficacy via overcoming poor penetration and enhancing accumulation of nanomedicines simultaneously. Here, we developed a near-infrared (NIR) light-triggered disintegratable delivery system (Lipo@ICG@CuS) composed of thermosensitive liposome, photosensitizer indocyanine green (ICG), and ultrasmall copper sulfide nanoparticles (CuS NPs), where ICG was embedded in the lipid bilayer and CuS NPs were encapsulated into the cavity of the liposome, respectively. Upon being irradiated by an 808 nm NIR laser, the local temperature of Lipo@ICG@CuS NPs is increased significantly, because of the photothermal capability of the loaded CuS NPs, and subsequently induces the structural collapse of thermosensitive liposomes to release the ICG and CuS NPs. The *in vitro* and *in vivo* results indicated that the as-prepared Lipo@ICG@CuS NPs could considerably prompt the CuS NPs to penetrate and accumulate deeply in tumors and obtained distinguished antitumor efficacy by combinatorial photodynamic therapy (PDT) and photothermal therapy (PTT). The current study provides a new strategy for solving the inherent dilemma of the long blood circulation but poor penetration and accumulation of large-sized NPs, as well as the deep penetration but easy clearance of small-sized NPs during the tumor therapy of nanomedicines.

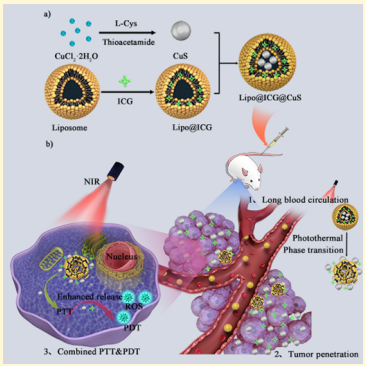

1. INTRODUCTION

Nanoparticles (NPs)-based drug delivery systems have drawn much attention in tumor therapy, because of the special physiochemical advantages, e.g., the enhanced permeability and retention (EPR) effect and long blood circulation time.[1−3] Generally, several aspects of the delivery processes are essential to be considered for improving the therapeutic efficacy, including blood circulation time, accumulation at the tumor site, penetration in the tumor tissue, internalization by tumor cells, and controllable drug release,[4,5] in which penetration is a big challenge for efficient drug delivery. Typically, nanocarriers can efficiently deliver the chemotherapeutics to the superficial layer of the tumor but are accompanied by the poor penetration efficiency for deep tumor tissues, which seriously limits the practical anticancer effects. This serious problem might be attributed to characteristics of the tumor, e.g., the abnormal tumor vasculature, dense composition of extracellular matrix (ECM), and the high interstitial fluid pressure.[6] So far, tremendous studies have been performed to overcome this problem.[7−11] For example, the ECM-degrading drugs or enzymes loaded onto the nanocarriers were developed to improve tumor penetration.[12−15] However, the enzyme activity might be susceptible to be interfered during circulation in the blood. Besides, the tumor microenvironment (TME) may be destroyed due to the enzymatic degradation of ECM, leading to tumor invasion or metastasis.[8] In addition, the nanomedicines might also be modified with tissue-penetrating peptides to improve the penetration efficiency,[16] but the inevitably complicated synthesis procedure and the high cost, in association with the objective peptides, seriously limit the practical application. More recently, the strategy to modulate the size of the NPs by utilizing the acidic TME has attracted much attention.[17,18] On the one hand, it could improve the

Received: August 3, 2022
Accepted: November 16, 2022
Published: November 23, 2022

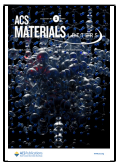

https://doi.org/10.1021/acsmaterialslett.2c00707
ACS Materials Lett. 2023, 5, 1−10

Scheme 1. (a) Preparation of Lipo@ICG@CuS NPs; (b) Proposed Working Mechanism of the Nanoparticles in Tumors

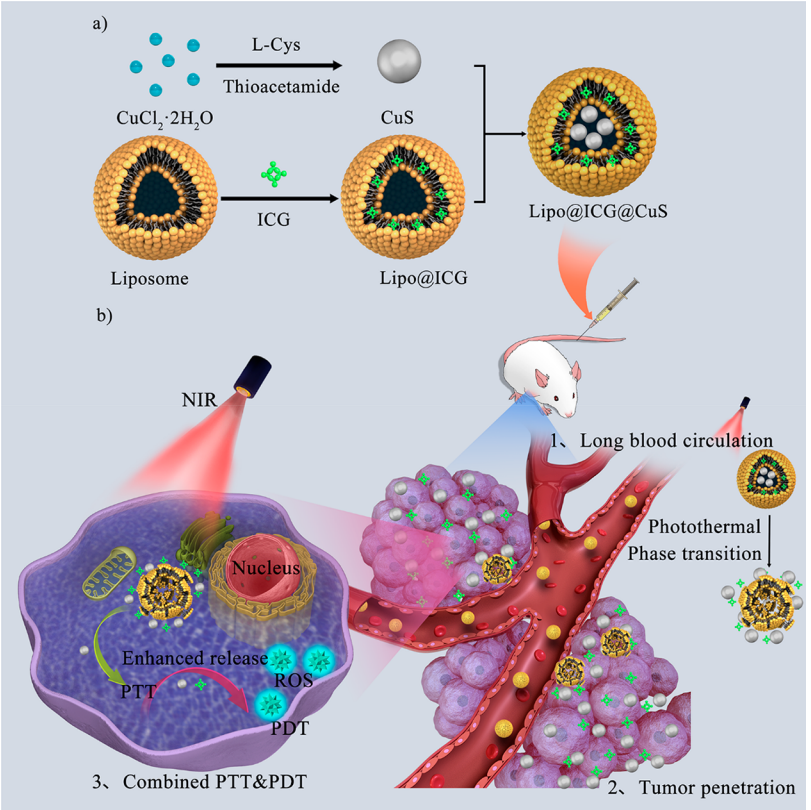

poor tumor penetration efficiency of the larger NPs by prolonging the circulation time. On the other hand, it could also address the dilemma of having good tumor penetration but being susceptible to clearance and short blood circulation of the smaller NPs.[19] However, modulation of the size of the NPs is largely dependent on the cleavage of the acidic-sensitive groups of the NPs, which is difficult to control, because of the response sensitivity in vivo. Consequently, there is an urgent need to explore novel strategies to endow the NPs with the improved tumor penetration and long blood circulation to enhance the antitumor effect considerably.

Liposomes are clinically used as drug carriers for cancer therapy because of special properties, similar to cell membranes, and the ability to load drugs regardless of the hydrophilicity or hydrophobicity.[20] Intelligent responsive liposomes such as ROS response and pH response have been designed to improve tumor therapeutic effects.[21−23] Thermosensitive liposomes composed of specific phospholipids could be disintegrated easily upon reaching the phase transition temperature, which could enhance the therapeutic outcome.[24] CuS nanomaterials, which are one class of important photothermal conversion nanoagents, could intensively absorb light and convert photon energy to local heating to efficiently kill the cancer cells and has attracted tremendous attention.[25,26] Indocyanine Green (ICG) can be applied for PDT and PTT, because of the ability to convert photoenergy into ROS and heat energy, and it also has been already approved by the United States Food and Drug Administration (US FDA) for clinical applications.[27,28]

Herein, we developed a new NIR-light-triggered disintegrable delivery system by loading the ultrasmall CuS NPs into larger thermosensitive liposomes to realize biocompatibility, prolonged circulation, and favorable penetration. In addition, ICG was loaded into the lipid layer of the liposome, which could exert a PDT effect and improve the tumor therapeutic effects through the combination with the PTT effect of CuS NPs (Scheme 1). The average size of the liposome was ∼167 nm, which was beneficial to circulate in the body. When exposed to an 808 nm NIR laser, the CuS NPs could absorb enough light energy to generate heat, which could result in the local hyperthermia and then damage the thermosensitive liposomes to release ICG and CuS NPs for deep penetration in the tumor tissue. The combined action of PDT of ICG with PTT of CuS NPs can kill cancer cells significantly. This nanosystem provided a strategy to address the dilemma of poor tissue penetration of large NPs and rapid clearance of small NPs and significantly improved the tumor therapeutic effect by combining PDT and PTT.

2. EXPERIMENTAL SECTION

2.1. Materials and Reagents. Dipalmitoylphosphatidylcholine (DPPC) and 1,2-distearoyl-*sn*-glycero-3-phosphoethanolamine-*N*-[methoxy(polyethylene glycol)-2000] (DSPE-PEG2000) were purchased from Shanghai Ponsure Biotech, Inc. Cholesterol was purchased from Shanghai Yuanye Bio-Technology Co., Ltd. Indocyanine green was purchased from J&K Scientific. Copper chloride dihydrate ($CuCl_2 \cdot 2H_2O$) was purchased from Aladdin. Fluorescein isothiocyanate (FITC) was purchased from Solarbio.

2.2. Cell Lines and Animals. The 4T1 and CHO cell lines were obtained from Cell Bank of Chinese Academy of Sciences. The cells were cultured at 37 °C with corresponding medium with 10% fetal bovine serum (FBS) added in a 5%

https://doi.org/10.1021/acsmaterialslett.2c00707
ACS Materials Lett. 2023, 5, 1−10

CO_2 humidified environment incubator (Thermo Scientific, USA).

The animals (Female Balb/c mice, 6−8 weeks) were fed under optimal conditions (25 °C and 55% of humidity). Tumor models were constructed by inoculating 2×10^6 cells into the subcutaneous of the mice. The treatment was started after the tumor size being ∼100 mm^3. All of the animal experiments that were performed met to the requirements of the Institutional Animal Care.

2.3. Synthesis of CuS NPs. The preparation of CuS NPs was performed as reported previously with slight modifications.[29] Briefly, 0.01 mmol cysteine (Cys) was added to the $CuCl_2 \cdot 2H_2O$ aqueous solution (1 mM, 100 mL) and stirred for 0.5 h to get a homogeneous system. An aqueous solution of thioacetamide (0.1 mmol) was added dropwise and reacted at 50 °C for 2 h, then centrifuged to collect CuS NPs. For the FITC labeling of CuS NPs, 1 mL of FITC-PEG-SH (10 mg/L, MW = 2000) and CuS NPs (5 mg/L) were mixed up and sonicated for 30 min. Next, the mixture was stirred overnight. The final product (CuS-FITC NPs) was obtained by centrifugation to get rid of the excess FITC-PEG-SH.[30]

2.4. Preparation of ICG-Loaded Liposome. The ICG-loaded liposome was prepared via the hydration of dry lipid films. Briefly, DPPC, cholesterol, DSPE-PEG2000, and ICG (molar ratio of 18:6:1.5:1) were dissolved in trichloromethane and then dried by rotary evaporators. Subsequently, PBS was used to hydrate the dried lipid film and then the obtained liposome was extrude using polycarbonate filters (400, 200, and 100 nm). The final solution was condensed by ultrafiltration device (30 kDa, Millipore).

2.5. Loading of CuS NPs. The Lipo@ICG@CuS NPs were obtained by fully hydrating the lipid film of Lipo@ICG with 2 mL of CuS NPs aqueous dispersion (2 mg/mL) for 1 h at 60 °C. In order to ensure efficient loading of CuS NPs into Lipo@ICG, the mixture was sonicated for 30 min. After centrifugating to remove the excess CuS NPs, PBS was used to resuspend the pellet. The final solution was extrude using polycarbonate filters (400, 200, and 100 nm). The loading content of CuS NPs was analyzed by ICP-MS.

2.6. Measurement of Responsive Release and Photothermal Performance. To test the response of the nanosystem, the release of CuS NPs and ICG response to NIR light irradiation was detected. Briefly, 2 mL of the solution (Lipo@ICG@CuS NPs) was irradiated with an 808 nm laser (0.8 W/cm^2, 10 min). The released CuS NPs and ICG were collected via centrifugation. The concentration of the CuS NPs and ICG were determined by inductively coupled plasma−mass spectroscopy (ICP-MS) and ultraviolet (UV) spectrometry, respectively.

Next, the photothermal performance of CuS NPs, Lipo@ICG NPs, Lipo@CuS NPs, and Lipo@ICG@CuS NPs was evaluated. Briefly, the 808 nm NIR laser (0.8 W/cm^2) was used to irradiate the aqueous suspensions (containing 50 μg/mL of CuS NPs) of different groups for 10 min. A high-precision thermocouple sensor was employed to record the temperature every minute when the experiment was being performed. The photothermal conversion efficiency was calculated according to the method constructed by Roper and co-workers.[31]

2.7. Penetration In Vitro. We constructed the 4T1-based multicellular spheroids according to the previous report with moderate modifications.[32] First, 96-well microplates were treated by 1% (w/v) agarose, and then 1×10^4 4T1 cells/well were seeded after agarose solution was solidified. Subsequently, the cells were cultured for 4−5 days getting multicellular spheroids with diameter of 300−400 μm. The images of cell spheroids were acquired by confocal laser scanning microscopy (CLSM) (Olympus, Model FV1200) after incubating with Lipo-DiI@CuS-FITC for 6 h. In addition, the penetration of Lipo@CuS under 808 nm NIR laser irradiation was also studied, the CuS NPs were labeled by FITC and irradiated by 808 nm NIR laser (0.8 W/cm^2, 10 min). The 4T1 multicellular spheres then were observed by CLSM.

2.8. Cellular Uptake. 5×10^4 4T1 cells were seeded into glass-bottom dishes and fresh medium (without FBS) containing Lipo-DiI@ICG@CuS NPs (16.9 μg/mL of CuS NPs) was added after cultivation for 48 h, and then incubated for another 6 h. Before staining with DAPI, the cells were washed with PBS and fixed with 4% paraformaldehyde solution for 20 min. The fluorescent images of cellular uptake were obtained by CLSM. And the flow cytometry (FACS Calibur) was used to quantify the fluorescence intensity of the NPs distributed in cells.

2.9. Intracellular ROS Detection. Intracellular ROS level was evaluated by using dichlorofluorescein diacetate (DCFH-DA). First, the cells were treated with the NPs for 6 h, then DCFH-DA (10 μM) was added and continued to incubate for another 20 min. Before observation with CLSM, the cells were exposed to 808 nm NIR laser irradiation (0.8 W/cm^2, 2 min). Flow cytometry was used to quantify the ROS level further and the procedures were the same as those described above, except that cells needed to be collected and analyzed using flow cytometry.

2.10. Biocompatibility and Cytotoxicity Evaluation. Biocompatibility and cytotoxicity were evaluated with a standard Resazurin method. Briefly, CHO cells or 4T1 cells (5×10^3 cells/well) were preseeded in 96-well microplates. The cells then were incubated with Lipo@ICG@CuS NPs at CuS NPs concentrations of 0.313, 0.625, 1.25, 2.5, and 5 μg/mL for 24 h. The fluorescence intensity of the supernatant was recorded (Ex = 540 nm, Em = 590 nm) after the Resazurin aqueous solution (20 μL, 0.5 mg/mL) was added and incubated for another 4 h. For cytotoxicity evaluation, the cells were incubated with Lipo@CuS NPs and Lipo@ICG@CuS NPs at the equivalent to CuS concentrations of 0.313, 0.625, 1.25, 2.5, and 5 μg/mL. Next, each well of the 96-well plates was exposed to 808 nm NIR laser irradiation (0.8 W/cm^2, 5 min). After another 12 h of incubation, the cytotoxicity was evaluated with the above standard Resazurin method. LIVE/DEAD assay was further studied to evaluate the cytotoxicity. After being treated with different NPs for 24 h, Calcein-AM (4 μM) and PI (4.5 μM) were added to stain the cells for 20 min and then observed by CLSM. For cell apoptosis assay, 4T1 cells were harvested and washed by PBS after being treated with different groups for 6 h. The cells then were incubated with Annexin V-FITC (5 μL) and PI (5 μL) for 15 min after resuspended in 100 μL of Annexin V binding buffer. The data were obtained using a flow cytometer.

2.11. Intratumoral Penetration. For intratumoral penetration, 20 μL of CuS-FITC loaded Lipo-DiI (CuS equivalent of 5 mg/kg) was injected into tumors of the mice directly. The mice were euthanized 2 h after injection, and the tumors were collected and embedded by OCT. Next, the cryosection of tumor with a thickness of 10 μm was fabricated (Leica Biosystems) and observed by CLSM. The untreated tumor tissue was used to offset the background signal of the tissues.

https://doi.org/10.1021/acsmaterialslett.2c00707
ACS Materials Lett. 2023, 5, 1−10

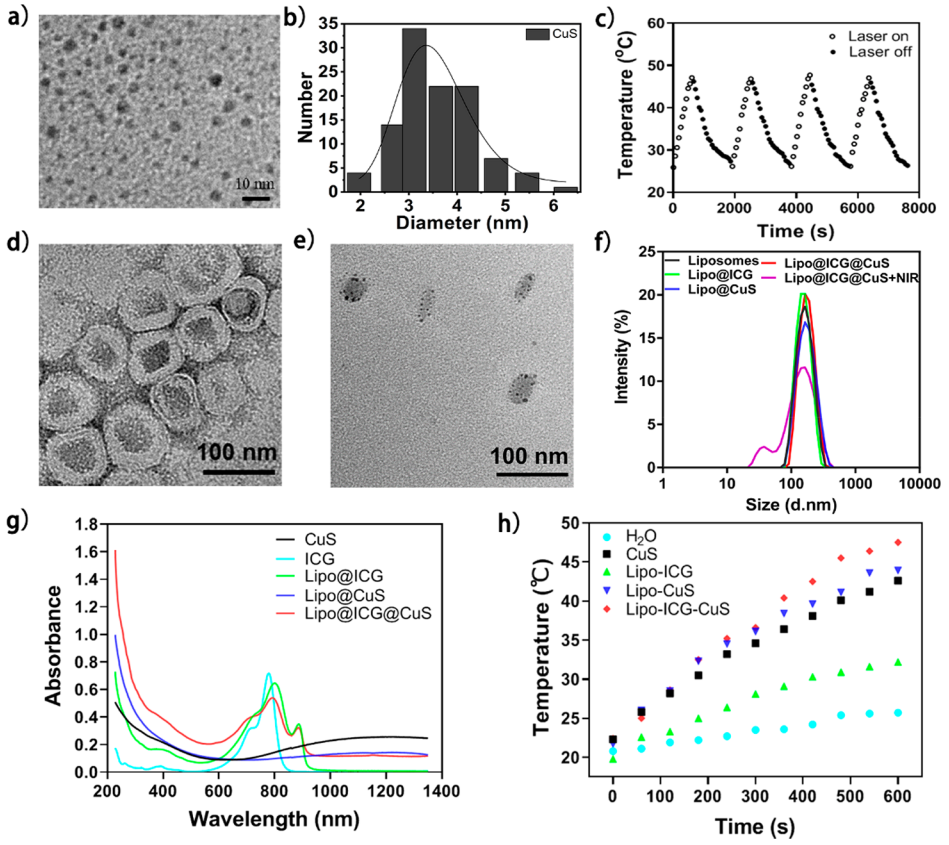

Figure 1. Characterization of the CuS NPs and liposome encapsulation. (a) TEM image of CuS NPs and (b) size distribution. (c) Photothermal cycling curves of the CuS NPs. (d,e)TEM images of Lipo@ICG@CuS with negative staining (panel (d)) and without negative staining (panel (e)). (f) Size distribution of Liposome, Lipo@ICG, Lipo@CuS, Lipo@ICG@CuS, and Lipo@ICG@CuS+NIR by DLS characterization. (g) UV spectra of the CuS, Lipo@ICG, Lipo@CuS, and Lipo@ICG@CuS. (h) Heating curves of H_2O, CuS, Lipo@ICG, Lipo@CuS, and Lipo@ICG@CuS irradiated by the 808 nm NIR laser (0.8 W/cm^2).

The penetration distance was determined using representative images, of which the fluorescent signal occupied a maximum area of tumor tissues. Furthermore, the intratumoral penetration was also studied under 808 nm NIR laser irradiation (1.0 W/cm^2, 10 min). The quantitative analysis of fluorescence intensity was performed by ImageJ software.

2.12. In Vivo and Ex Vivo Imaging. To trace the biodistribution of the NPs in vivo, Lipo-DiI@CuS NPs were injected into the mice via the tail vein. The mice then were imaged using an imaging system (IndiGo 2) at the setting time points.

To analyze the biodistribution, CuS-FITC loaded liposomes were administered into 4T1 tumor bearing mice via tail vein injection. The mice were sacrificed at 24 h postadministered and major organs (heart, liver, spleen, lung, kidney) and tumors were imaged. The IndiGo software was employed to analyze quantitatively the accumulation and distribution of the NPs.

2.13. In Vivo Photothermal and Photodynamic Therapy and Histological Evaluation. In this study, Balb/c mice bearing tumors were divided into four random groups: PBS, Lipo@CuS NPs (5 mg/kg CuS), Lipo@ICG NPs (1.84 mg/kg ICG), and Lipo@ICG@CuS NPs (5 mg/kg CuS, 1.84 mg/kg ICG). The treatment was performed when the tumor grew to ∼100 mm^3, and the mice were medicated on days 0, 3, and 6 via the tail vein. Twenty four hours (24 h) after administration, the tumor site was exposed to 808 nm NIR laser irradiation for 10 min (1.0 W/cm^2). Before sacrifice, the tumor size and body weight must be recorded every 2 days. H&E staining of major organs and tumor tissues proceeded after treatment for 21 days. First, the tumors were fixed in 4% paraformaldehyde before embedding into paraffin. The tumors then were sectioned into slices at a thickness of 5 μm. Finally, these slices were stained with hematoxylin and eosin for further pathological analysis. Besides, TUNEL Apoptosis Assay Kit was used to evaluate the apoptosis of tumor tissues. The procedure was performed according to the manufacturer instructions (Beyotime Biotechnology).

2.14. Statistical Analysis. Statistical analysis between two groups of independent data relied on Student's Unpaired *t*-test. One-way or two-way analysis of variance was required if there were multiple comparisons. Differences were regarded as statistically significant at (*) $p < 0.05$, (**) $p < 0.01$, and (***) $P < 0.001$. Results were shown as the mean ± standard deviation (SD).

3. RESULTS AND DISCUSSION

3.1. Synthesis and Characterization of the Lipo@ICG@CuS NPs. To obtain the Lipo@ICG@CuS NPs, well-dispersed ultrasmall CuS NPs with the average size of ∼3.1 nm were synthesized based on the previous report with minor modifications[29] (Figures 1a and 1b). The ultrasmall size of CuS NPs was beneficial to penetrate into tumor tissue deeply. Moreover, CuS NPs exhibited good NIR photothermal effect during four irradiation/cooling cycles (Figure 1c), with a

https://doi.org/10.1021/acsmaterialslett.2c00707
ACS Materials Lett. 2023, 5, 1−10

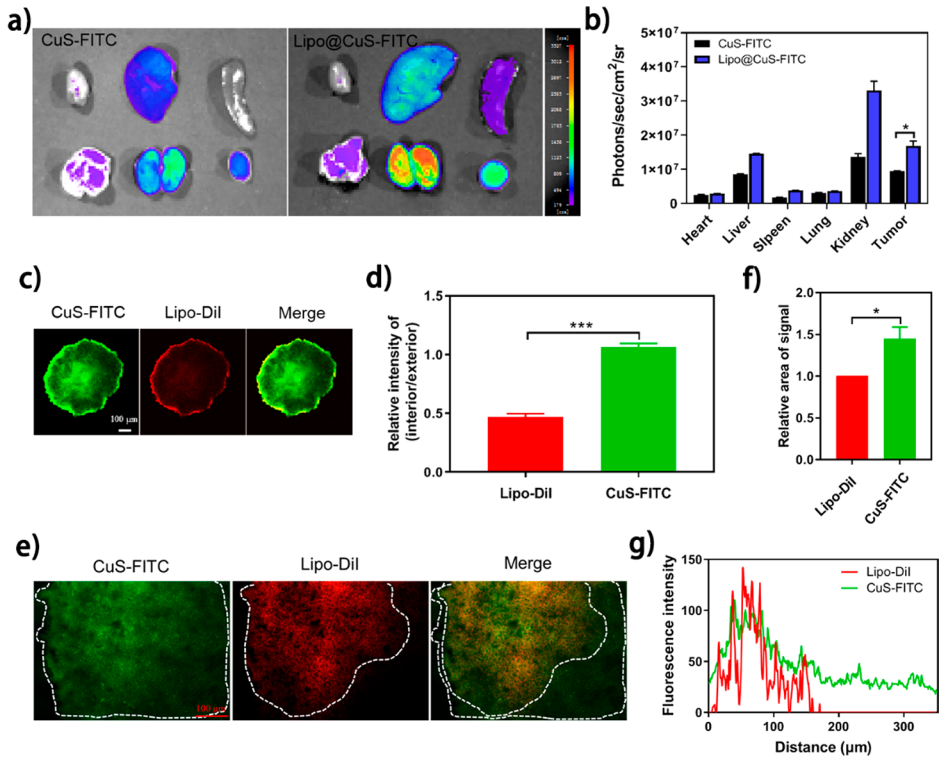

Figure 2. Characterization of distribution and penetration. (a) Accumulation of CuS-FITC NPs and Lipo@CuS-FITC NPs after intravenous injection for 24 h (n = 3). (b) Quantitative analysis of biodistribution of CuS-FITC NPs and Lipo@CuS-FITC NPs in tumor and major organs. (c) Penetration of Lipo-DiI@CuS-FITC NPs through 4T1 tumor spheroids. (d) Quantitative analysis of penetration of Lipo-DiI@CuS-FITC NPs in spheroids by using a custom-made formula A_0/A_1 (A_0 and A_1 represent the mean fluorescence intensity of the areas distant from center within 50 μm and outside to inside within 20 μm, respectively.) (e) Distribution of Lipo-DiI@CuS-FITC NPs in tumor tissues after intratumoral injection (n = 3). (f, g) Image-based quantitative analysis of distribution area (panel (f)) and penetration distance of intratumoral injected Lipo-DiI@CuS-FITC NPs (panel (g)), respectively.

photothermal conversion efficiency of 28.1% (see Figure 1c, as well as Figure S1 in the Supporting Information).

Considering the widespread potential applications of ICG for PDT and CuS NPs for PTT in cancer therapy, the nanoscaled Lipo@ICG@CuS containing liposome, ICG, and the CuS NPs were synthesized. Compared with the TEM image of liposome alone (Figure 1d), the dark CuS NPs could be clearly observed from the TEM image of Lipo@ICG@CuS NPs (Figure 1e), suggesting the successful loading of CuS NPs into liposomes. The encapsulation efficacy of CuS NPs was determined as 16.9% through ICP-MS analysis. Dynamic light scattering (DLS) analysis revealed that Lipo@ICG@CuS NPs had a narrow size distribution range, and the mean diameter was 167 nm, increasing by 22 nm than that of Lipo@ICG NPs. However, the disintegration of the liposomes generated some debris and the mean diameter dropped to 110 nm upon 808 nm NIR laser irradiation (Figure 1f). To further prove the successful loading of CuS NPs and ICG in the liposome, we recorded and compared the ultraviolet-visible light near-infrared (UV-vis-NIR) absorption spectrum of different samples. From the results shown in Figure 1g, Lipo@CuS NPs show a remarkable absorption similar to CuS NPs between 800 nm and 1350 nm. Lipo@ICG NPs exhibit the remarkable absorption of ICG (600−850 nm). In the spectrum of Lipo@ICG@CuS NPs, the absorptions of CuS NPs and ICG can be clearly observed, indicating the successful loading of CuS NPs and ICG into the liposome. Considering the major contribution of the heating performance during the process of PTT, the photothermal effect of Lipo@ICG@CuS NPs was determined subsequently. Upon irradiated by 808 nm NIR laser, the temperature of the Lipo@ICG@CuS NPs dispersion increased by ∼25 °C, slightly higher than that of CuS NPs alone (20 °C) and Lipo@CuS NPs (22 °C) (Figure 1h), which may be attributed to the certain photothermal capacity of ICG.[33,34] Furthermore, TEM observation reveals that the thermosensitive liposome disintegrated rapidly and released the cargoes due to the good photothermal effect (Figure S2 in the Supporting Information). In addition, the drug release was also evaluated upon NIR light irradiation, the accumulative release of the CuS NPs and ICG was 44.9% and 55.2%, respectively, which was significantly enhanced more than that without NIR light irradiation (6.7% and 9.7%, respectively). This might be attributed to the rapid disintegration of the liposomes induced by the PTT effect (Figure S3 in the Supporting Information). All these results indicated that the Lipo@ICG@CuS NPs with good photothermal effect were synthesized successfully.

3.2. Combined Effects of the Disintegratable Nanosystem. To study the enhanced penetration and retention capacity, we studied the combined effects originated from this disintegratable nanosystem. As one type of important small sized NPs widely studied in nanomedicines, ultrasmall CuS NPs showed short blood circulation time and were easily cleared.[35] Therefore, the tumor accumulation of ultrasmall CuS NPs was expected to be increased by prolonging the circulation time. As such, the biodistribution of NPs in the tumor sites and major organs was visualized via an IndiGo in vivo imaging system after intravenous (i.v.) administration to

https://doi.org/10.1021/acsmaterialslett.2c00707
ACS Materials Lett. 2023, 5, 1−10

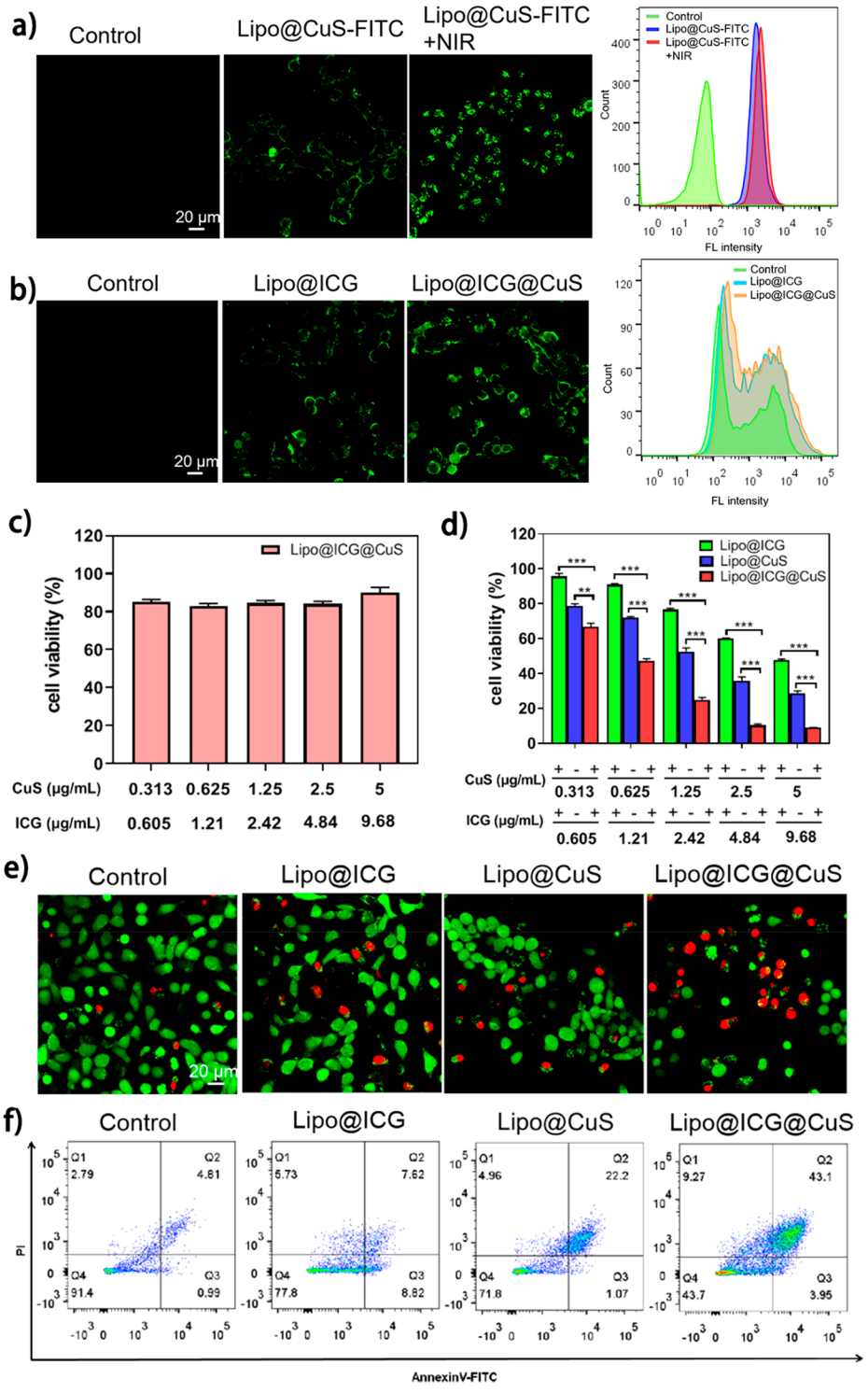

Figure 3. Cellular uptake and PTT&PDT-induced cell killing ability. (a) Cellular uptake of Lipo@CuS-FITC with or without 808 nm irradiation at 0.8 W/cm^2 and flow cytometry analysis. (b) Detection of intracellular ROS after treated with Lipo@ICG and Lipo@CuS@ICG and flow cytometry analysis. (c) Biocompatibility of CHO cells treated with different concentration of Lipo@ICG@CuS. (d) Cytotoxicity of different concentration of Lipo@ICG, Lipo@CuS, and Lipo@ICG@CuS. (e) Live (green)/dead (red) staining of 4T1 cells. (f) Apoptosis of 4T1 cells analyzed via flow cytometry.

the mice. Figure 2a indicates that both Lipo@CuS-FITC NPs and CuS-FITC NPs accumulated at tumor sites obviously. Moreover, the fluorescence intensity of Lipo@CuS-FITC NPs is approximately 1.8-fold higher than that of CuS-FITC NPs within tumors (Figure 2b). This result directly reveals that the as-prepared disintegratable delivery system can significantly prolong the blood circulation time and enhance the accumulation of CuS NPs at the tumor site.

3.3. Penetration of the Lipo@ICG@CuS-FITC NPs. Poor penetration is a vital factor for inadequate accumulation of NPs in the tumor and usually leads to an unsatisfactory therapeutic efficacy. It is well-known that multicellular tumor spheroids

https://doi.org/10.1021/acsmaterialslett.2c00707
ACS Materials Lett. 2023, 5, 1−10

have been used for studying the in vitro penetration of nanomedicines as the well-established model. Thus, we explored the penetration ability of Lipo@ICG@CuS-FITC NPs labeled by DiI throughout 4T1 multicellular tumor spheroids. Following incubation with Lipo-DiI@ICG@CuS-FITC NPs, from the 3D reconstructed CLSM images of spheroids (Figure 2c), liposome labeled by DiI are mainly located around the margin of the tumor spheroids. In strong contrast, CuS-FITC NPs can deeply penetrate throughout the entire spheroids and even in the center region. From the quantitative analysis shown in Figure 2d, the relative fluorescence intensity of CuS NPs was obviously stronger than that of liposomes (by ∼2-fold), indicating that CuS NPs were prone to penetrating to the center regions more easily. The tissue penetration ability of liposomes was limited, which may be attributed to "the binding site barrier effect", because their membrane could fuse with extravascular tumor cells.[36] Furthermore, we explored the distribution of Lipo@ICG@CuS-FITC NPs in tumor tissue via intratumoral injection to deeply understand the penetration ability. From Figure 2e, the fluorescence signal between liposomes and CuS NPs did not overlap perfectly in the tumor tissue.

In other words, the penetration distance of CuS NPs is different to that of the liposomes within tumors. From the image-based quantification analysis results, CuS NPs exhibit nearly a 1.5-fold greater distribution, in comparison with liposomes (Figures 2f and 2g). Furthermore, the penetration under NIR light irradiation was also explored in vitro and in vivo. The in vitro results showed that the penetration depth of the Lipo@CuS-FITC NPs was only ∼45 μm, while the depth deepened markedly upon the NIR light irradiation (∼85 μm), which might be ascribed to the release of CuS NPs from the disintegrated liposomes (Figure S4a in the Supporting Information). The line profile analysis also demonstrated that the fluorescence mainly located at the periphery of the multicellular tumor spheroids at the depth of 85 μm without NIR light irradiation, while the fluorescence almost distributed throughout the multicellular spheroids under NIR light irradiation (Figure S4b in the Supporting Information). The results of penetration in tumor tissue indicated that CuS NPs showed nearly 2-fold greater distribution in comparison with liposomes, which was considerable greater than that without NIR light irradiation due to CuS NPs release (see Figures S4c and S4d in the Supporting Information). These results implied that CuS NPs could be released from liposome and penetrated into deep tumor tissue further, especially under NIR light irradiation.

3.4. Cellular Uptake and Cytotoxicity. Subsequently, the cellular uptake efficiency of Lipo@ICG@CuS NPs was evaluated. After co-incubation of 4T1 cells with Lipo@ICG@CuS NPs labeled by DiI, we first checked whether the Lipo@ICG@CuS NPs could be efficiently internalized. The CLSM images displayed strong fluorescent signal of Lipo@ICG@CuS NPs labeled by DiI within the cytoplasm of 4T1 cells (Figure S5a in the Supporting Information), revealing the efficient cellular uptake. This result was further confirmed by the stronger fluorescence intensity of Lipo@ICG@CuS NPs using the flow cytometry analysis (Figure S5b in the Supporting Information). Besides, after irradiated by an 808 nm NIR laser, the Lipo@CuS-FITC NPs showed moderate stronger fluorescent signal than without irradiation (Figure 3a), suggesting that the photothermal effect could prompt the release of CuS NPs, which was further confirmed by the higher fluorescent intensity of NIR laser irradiation treatment group in the flow cytometric histogram. And it was also proved by fluorescence spectrophotometer analysis, in which the fluorescence intensity of Lipo@CuS-FITC NPs with NIR laser irradiation was stronger than that without NIR laser irradiation (Figure S6 in the Supporting Information). This phenomenon may be ascribed to the fact that the CuS NPs loaded into liposome just absorb part of the excitation light while the quickly released CuS NPs from Lipo@ICG@CuS NPs under 808 nm NIR laser irradiation can enhance the light absorption and the corresponding emission intensity.[37,38] The high-efficiency cellular uptake provided a solid foundation for exerting the PTT effect of CuS and PDT effect of ICG. The intracellular ROS level then was evaluated using a DCFH-DA probe. From the CLSM images shown in Figure 3b, the fluorescent intensity of the 4T1 cells treated by Lipo@ICG@CuS NPs under NIR laser irradiation is considerably stronger than that of the Lipo@ICG NPs treatment group, suggesting the higher intracellular ROS level of Lipo@ICG@CuS NPs + NIR treatment group. Meanwhile, stronger intracellular ROS level of Lipo@ICG@CuS NPs than Lipo@ICG NPs was also demonstrated by the flow cytometric quantification analysis. These results could be ascribed to a great deal of release of ICG from the disintegration of liposome triggered by the photothermal effect of CuS NPs. The cytocompatibility of Lipo@ICG@CuS NPs was assessed through a standard Resazurin Method. Figure 3c shows that, after being co-incubated with different concentrations of Lipo@ICG@CuS NPs, the viability of CHO normal cells is still maintained above 80%, suggesting the good cytocompatibility of Lipo@ICG@CuS NPs. The in vitro PDT and PTT effects of the Lipo@ICG@CuS NPs then were evaluated. From the data shown in Figure 3d, after being treated with Lipo@ICG@CuS NPs under 808 nm NIR laser irradiation, the viability of 4T1 cancer cells is much lower than those of the Lipo@ICG NPs and Lipo@CuS NPs treatment groups. For example, after being treated by 5 μg/mL of Lipo@ICG@CuS NPs under 5 min irradiation of 808 nm NIR laser, the viability of 4T1 cells is <10%, which is much lower than those of Lipo@ICG NPs (45%) and Lipo@CuS NPs (30%) treatment groups under same conditions. These data implied the combined therapeutic effects of Lipo@ICG@CuS NPs. The Calcien AM and propidium iodide live/dead cell staining assay results were consistent with that of the cytotoxicity test, the Lipo@ICG@CuS NPs treatment group exhibited the strongest red fluorescence, indicating the strongest cytotoxic effect on 4T1 cells (Figure 3e). Moreover, the therapeutic effect of Lipo@ICG@CuS NPs was further confirmed by flow cytometry analysis. From the results shown in Figure 3f, after treated by Lipo@ICG NPs, Lipo@CuS NPs, and Lipo@ICG@CuS NPs under NIR laser irradiation, the content of apoptotic and necrotic cells was determined to be 22.2%, 28.2%, and 56.3%, respectively, revealing the strongest apoptosis and necrosis inducing effects of Lipo@ICG@CuS NPs. All of the above proved that the as-prepared Lipo@ICG@CuS NPs can combine the PTT effect of CuS and PDT effect of ICG to significantly enhance the antitumor efficacy.

3.5. Tumor Accumulation and Antitumor Efficacy. Following the evaluation of antitumor effect in vitro, we subsequently investigated the potential in vivo antitumor effect of the Lipo@ICG@CuS NPs.

First, the time-dependent accumulation of Lipo@ICG@CuS NPs at the tumor site was tracked by an imaging system after

https://doi.org/10.1021/acsmaterialslett.2c00707
ACS Materials Lett. 2023, 5, 1−10

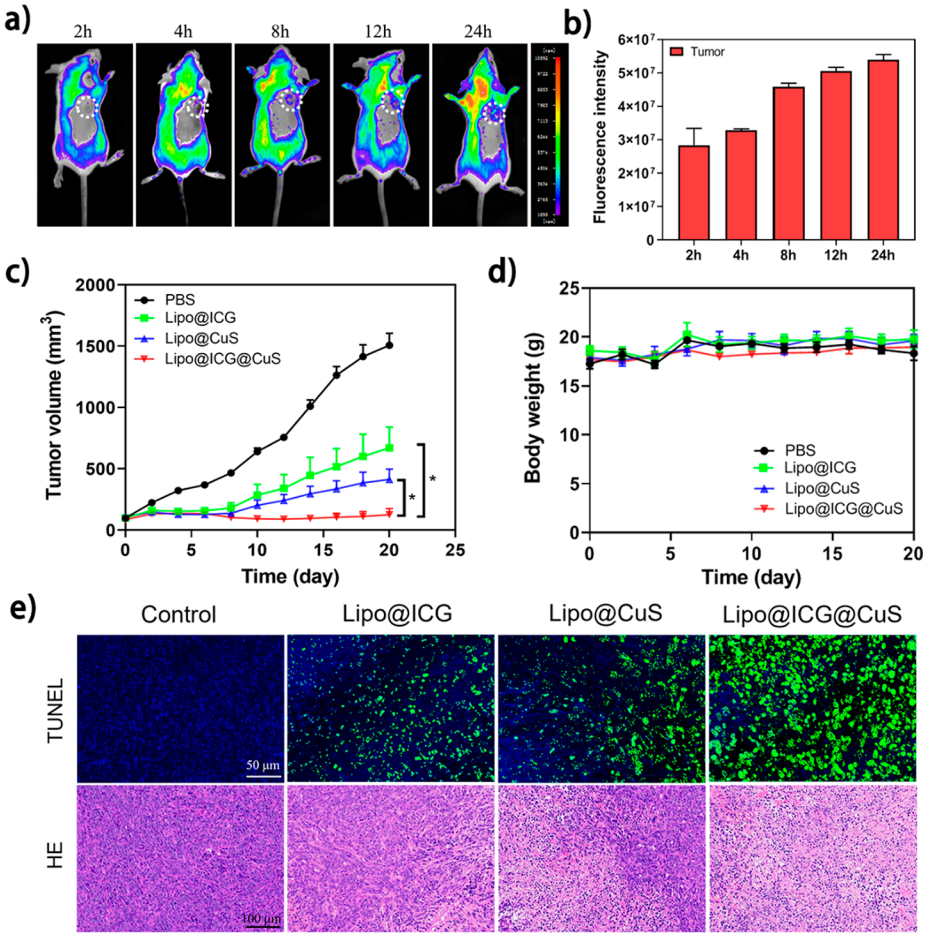

Figure 4. Tumor accumulation and antitumor activity in vivo. (a) Imaging of Balb/c mice bearing tumor (white circle) with time, following i.v. administration of Lipo@ICG@CuS NPs labeled by DiI. (b) Quantitative analysis of fluorescence intensity of Lipo@ICG@CuS NPs labeled by DiI at the tumor site with time. (c) Changes of tumor volume after treated by different groups (n = 8). (d) Body weight changes with different treatments. (e) TUNEL staining (upper panels) and H&E staining (lower panels) of tumor tissues after being treated with different groups.

i.v. administration. From the results shown in Figure 4a, the efficient accumulation of Lipo@ICG@CuS NPs in tumor areas (white circle) can be clearly observed over time. From the data shown in Figure 4b, in comparison with the Lipo-DiI fluorescence signal intensity at 2 h postinjection, the signal intensity exhibits ∼1.9-fold increases at 24 h post-injection, clearly revealing the efficient accumulation of Lipo@ICG@CuS NPs at the tumor site.

Subsequently, combinatorial antitumor effect of Lipo@ICG@CuS NPs was evaluated in vivo. Briefly, Balb/c mice bearing tumors were divided into four random groups: PBS, Lipo@ICG NPs (1.84 mg/kg ICG), Lipo@CuS NPs (5 mg/kg CuS), and Lipo@ICG@CuS NPs (1.84 mg/kg ICG, 5 mg/kg CuS). Considering the efficient tumor accumulation of Lipo@ICG@CuS NPs at 24 h, the tumors were exposed to 808 nm NIR laser irradiation (1.0 W/cm^2) for 10 min after 24 h of i.v. administration. The tumor size and body weight must be recorded every 2 days. As shown in Figure 4c, tumor growth was significantly restrained after treated with Lipo@ICG NPs and Lipo@CuS NPs. Notably, the Lipo@ICG@CuS NPs exhibit much stronger therapeutic efficacy than other groups, the tumor growth in this group is almost completely inhibited. This can be mainly attributed to the thermosensitive disintegration of liposome to release CuS and ICG due to the photothermal effect of CuS NPs, which was conducive to efficient penetration of CuS NPs and ICG into deep tumor tissue and the remarkable combined effect of PTT of CuS and PDT of ICG. There were no obvious changes of body weight in four groups, indicating good biosafety of the nanosystems (Figure 4d). In addition, the H&E staining results showed that tumor tissues treated by Lipo@ICG@CuS NPs were damaged seriously, compared with other groups. Furthermore, TUNEL staining was performed, and the results showed that the Lipo@ICG@CuS NPs group exhibited much stronger positive signal than other groups, indicating that the combined effect of PTT and PDT could remarkably induce the apoptosis (Figure 4e). Moreover, images of H&E staining of major organs revealed that there was no apparent systemic toxicity induced by Lipo@ICG NPs, Lipo@CuS NPs, and Lipo@ICG@CuS NPs after 21 days of treatment (see Figure S7 in the Supporting Information). Taken together, the as-prepared Lipo@ICG@CuS NPs can efficiently combine the PTT and PDT effects to significantly inhibit the tumor development, because of the enhanced accumulation and penetration of the CuS NPs at the tumor sites triggered by NIR light irradiation.

4. CONCLUSIONS

In summary, a NIR light-responsive disintegratable delivery system (Lipo@ICG@CuS) was developed that can endow ultrasmall CuS NPs with long blood circulation and release the

https://doi.org/10.1021/acsmaterialslett.2c00707
ACS Materials Lett. 2023, 5, 1−10

NPs at the tumor site to improve the accumulation and penetration in the tumor. The liposome collapsed rapidly, triggered by the photothermal effect of CuS NPs upon NIR light irradiation at the tumor site, and the ultrasmall CuS NPs and ICG were released, resulting in the improved accumulation and deep tumor penetration of CuS NPs and ICG. The enhanced antitumor effect *in vivo* was achieved by combining PTT and PDT under single 808 nm light irradiation. This provides a strong inspiration to develop the novel multifunctional nanomedicines with long blood circulation and deep penetration for the multimodal treatment of human cancer.

■ ASSOCIATED CONTENT

Supporting Information

The Supporting Information is available free of charge at https://pubs.acs.org/doi/10.1021/acsmaterialslett.2c00707.

Photothermal effect of CuS NPs, TEM analysis of the Lipo@ICG@CuS irradiated by an 808-nm NIR laser, confocal imaging and flow cytometry analysis of cellular uptake, fluorscence emission spectra of Lipo@CuS-FITC and Lipo@CuS-FITC+NIR, and H&E staining images of major organs (PDF)

■ AUTHOR INFORMATION

Corresponding Authors

Yuming Guo − *School of Chemistry and Chemical Engineering, Henan Normal University, Xinxiang, Henan 453007, China;* orcid.org/0000-0002-2351-4456; Email: guoyuming@htu.edu.cn

Xiaoming Ma − *Key Laboratory of Green Chemical Media and Reactions, Ministry of Education, Henan Normal University, Xinxiang, Henan 453007, China;* orcid.org/0000-0002-3209-4182; Email: mxm@htu.edu.cn

Authors

Fangli Gao − *School of Chemistry and Chemical Engineering, Henan Normal University, Xinxiang, Henan 453007, China*

Liting Jiang − *Key Laboratory of Green Chemical Media and Reactions, Ministry of Education, Henan Normal University, Xinxiang, Henan 453007, China*

Jie Zhang − *School of Chemistry and Chemical Engineering, Henan Normal University, Xinxiang, Henan 453007, China*

Yi Chang − *School of Chemistry and Chemical Engineering, Henan Normal University, Xinxiang, Henan 453007, China;* orcid.org/0000-0002-9432-5492

Weihua Gao − *School of Chemistry and Chemical Engineering, Henan Normal University, Xinxiang, Henan 453007, China*

Lina Ding − *Key Laboratory of Green Chemical Media and Reactions, Ministry of Education, Henan Normal University, Xinxiang, Henan 453007, China*

Guanglei Ma − *Key Laboratory of Green Chemical Media and Reactions, Ministry of Education, Henan Normal University, Xinxiang, Henan 453007, China*

Complete contact information is available at: https://pubs.acs.org/10.1021/acsmaterialslett.2c00707

Author Contributions

[▽]F. Gao and L. Jiang contributed equally to this work. CRediT: **Fangli Gao**: Conceptualization, Formal analysis, Investigation, Methodology, Writing-original draft. **Liting Jiang**: Conceptualization, Methodology, Investigation, Data curation. **Jie Zhang**: Supervision, Resources. **Yi Chang**: Supervision, Resources, Funding acquisition. **Weihua Gao**: Investigation, Resources. **Lina Ding**: Conceptualization, Resources. **Guanglei Ma**: Conceptualization, Resources. **Xiaoming Ma**: Conceptualization, Resources, Supervision, Writing-review and editing, Funding acquisition, Project administration. **Yuming Guo**: Conceptualization, Resources, Supervision, Writing-review and editing, Funding acquisition, Project administration.

Notes

The authors declare no competing financial interest.

■ ACKNOWLEDGMENTS

This work was financially supported by the National Natural Science Foundation of China (Nos. 21771058 and 21877027), the Natural Science Foundation of Henan (No. 212300410009), and the Program for Science & Technology Innovation Talents in Universities of Henan Province (No. 23HASTIT002).

■ REFERENCES

(1) Fang, J.; Islam, W.; Maeda, H. Exploiting the dynamics of the EPR effect and strategies to improve the therapeutic effects of nanomedicines by using EPR effect enhancers. *Adv. Drug Delivery Rev.* **2020**, *157*, 142−160.

(2) Liu, F.; Cong, Y.; Qi, G.; Ji, L.; Qiao, Z.; Wang, H. Near-Infrared Laser-Driven in Situ Self-Assembly as a General Strategy for Deep Tumor Therapy. *Nano Lett.* **2018**, *18*, 6577−6584.

(3) Wilhelm, S.; Tavares, A. J.; Dai, Q.; Ohta, S.; Audet, J.; Dvorak, H.; Chan, W. C. W. Analysis of nanoparticle delivery to tumours. *Nat. Rev. Mater.* **2016**, *1*, 16014.

(4) Sun, Q.; Zhou, Z.; Qiu, N.; Shen, Y. Rational Design of Cancer Nanomedicine: Nanoproperty Integration and Synchronization. *Adv. Mater.* **2017**, *29*, 1606628.

(5) Xu, C.; Sun, Y.; Yu, Y.; Hu, M.; Yang, C.; Zhang, Z. A Sequentially Responsive and Structure-transformable Nanoparticle with Comprehensively Improved 'CAPIR cascade' for Enhanced Antitumor Effect. *Nanoscale* **2019**, *11*, 1177−1194.

(6) Zhu, Y.; Song, Y.; Cao, Z.; Dong, L.; Lu, Y.; Yang, X.; Wang, J. Magnetically Actuated Active Deep Tumor Penetration of Deformable Large Nanocarriers for Enhanced Cancer Therapy. *Adv. Funct. Mater.* **2021**, *31*, 2103655.

(7) Li, Z.; Shan, X.; Chen, Z.; Gao, N.; Zeng, W.; Zeng, X.; Mei, L. Applications of Surface Modification Technologies in Nanomedicine for Deep Tumor Penetration. *Adv. Sci.* **2021**, *8*, 2002589.

(8) Ding, J.; Chen, J.; Gao, L.; Jiang, Z.; Zhang, Y.; Li, M.; Xiao, Q.; Lee, S.; Chen, X. Engineered nanomedicines with enhanced tumor penetration. *Nano Today* **2019**, *29*, 100800.

(9) Matsumoto, Y.; Nichols, J.; Toh, K.; Nomoto, T.; Cabral, H.; Miura, Y.; Christie, R.; Yamada, N.; Ogura, T.; Kano, M.; Matsumura, Y.; Nishiyama, N.; Yamasoba, T.; Bae, Y.; Kataoka, K. Vascular bursts enhance permeability of tumour blood vessels and improve nanoparticle delivery. *Nat. Nanotechnol.* **2016**, *11*, 533−538.

(10) Li, Y.; Chen, M.; Yao, B.; Lu, X.; Song, B.; Vasilatos, S.; Zhang, X.; Ren, X.; Yao, C.; Bian, W.; Sun, L. Dual pH/ROS-Responsive Nanoplatform with Deep Tumor Penetration and Self-Amplified Drug Release for Enhancing Tumor Chemotherapeutic Efficacy. *Small* **2020**, *16*, 2002188.

(11) Zhang, Z.; Wang, H.; Tan, T.; Li, J.; Wang, Z.; Li, Y. Rational Design of Nanoparticles with Deep Tumor Penetration for Effective Treatment of Tumor Metastasis. *Adv. Funct. Mater.* **2018**, *28*, 1801840.

(12) Xu, F.; Huang, X.; Wang, Y.; Zhou, S. A Size-Changeable Collagenase-Modified Nanoscavenger for Increasing Penetration and Retention of Nanomedicine in Deep Tumor Tissue. *Adv. Mater.* **2020**, *32*, 1906745.

(13) Han, H.; Hou, Y.; Chen, X.; Zhang, P.; Kang, M.; Jin, Q.; Ji, J.; Gao, M. Metformin-Induced Stromal Depletion to Enhance the

Penetration of Gemcitabine-Loaded Magnetic Nanoparticles for Pancreatic Cancer Targeted Therapy. *J. Am. Chem. Soc.* **2020**, *142*, 4944−4954.
(14) Chen, X.; Jia, F.; Li, Y.; Deng, Y.; Huang, Y.; Liu, W.; Jin, Q.; Ji, J. Nitric oxide-induced stromal depletion for improved nanoparticle penetration in pancreatic cancer treatment. *Biomaterials* **2020**, *246*, 119999.
(15) Cui, T.; Yan, Z.; Qin, H.; Sun, Y.; Ren, J.; Qu, X. A Sequential Target-Responsive Nanocarrier with Enhanced Tumor Penetration and Neighboring Effect In Vivo. *Small* **2019**, *15*, 1903323.
(16) Lu, L.; Zhao, X.; Fu, T.; Li, K.; He, Y.; Luo, Z.; Dai, L.; Zeng, R.; Cai, K. An iRGD-conjugated prodrug micelle with blood-brain-barrier penetrability for anti-glioma therapy. *Biomaterials* **2020**, *230*, 119666.
(17) Zhang, Z.; Wang, T.; Yang, R.; Fu, S.; Guan, L.; Hou, T.; Mu, W.; Pang, X.; Liang, S.; Liu, Y.; Zhang, N. Small Morph Nanoparticles for Deep Tumor Penetration via Caveolae-Mediated Transcytosis. *ACS Appl. Mater. Interfaces* **2020**, *12*, 38499−38511.
(18) Yu, W.; Liu, R.; Zhou, Y.; Gao, H. Size-Tunable Strategies for a Tumor Targeted Drug Delivery System. *ACS Central Sci.* **2020**, *6*, 100−116.
(19) Wang, Z.; Ju, Y.; Ali, Z.; Yin, H.; Sheng, F.; Lin, J.; Wang, B.; Hou, Y. Near-infrared light and tumor microenvironment dual responsive size-switchable nanocapsules for multimodal tumor theranostics. *Nat. Commun.* **2019**, *10*, 1−12.
(20) Filipczak, N.; Pan, J.; Yalamarty, S.; Torchilin, V. Recent advancements in liposome technology. *Adv. Drug Delivery Rev.* **2020**, *156*, 4−22.
(21) Cheng, X.; Gao, J.; Ding, Y.; Lu, Y.; Wei, Q.; Cui, D.; Fan, J.; Li, X.; Zhu, E.; Lu, Y.; Wu, Q.; Li, L.; Huang, W. Multi-Functional Liposome: A Powerful Theranostic Nanocclatform Enhancing Photodynamic Therapy. *Adv. Sci.* **2021**, *8*, 2100876.
(22) Large, D.; Abdelmessih, R.; Fink, E.; Auguste, D. Liposome composition in drug delivery design, synthesis, characterization, and clinical application. *Adv. Drug Delivery Rev.* **2021**, *176*, 113851.
(23) Lou, J.; Best, M. Reactive Oxygen Species-Responsive Liposomes via Boronate-Caged Phosphatidylethanolamine. *Bioconjugate Chem.* **2020**, *31*, 2220−2230.
(24) Xiong, X.; Xu, Z.; Huang, H.; Wang, Y.; Zhao, J.; Guo, X.; Zhou, S. A NIR light triggered disintegratable nanoplatform for enhanced penetration and chemotherapy in deep tumor tissues. *Biomaterials* **2020**, *245*, 119840.
(25) Li, N.; Sun, Q.; Yu, Z.; Gao, X.; Pan, W.; Wan, X.; Tang, B. Nuclear-Targeted Photothermal Therapy Prevents Cancer Recurrence with Near-Infrared Triggered Copper Sulfide Nanoparticles. *ACS Nano* **2018**, *12*, 5197−5206.
(26) Wu, X.; Suo, Y.; Shi, H.; Liu, R.; Wu, F.; Wang, T.; Ma, L.; Liu, H.; Cheng, Z. Deep-Tissue Photothermal Therapy Using Laser Illumination at NIR-IIa Window. *Nano-Micro Lett.* **2020**, *12*, 1−13.
(27) Liu, C.; Cao, Y.; Cheng, Y.; Wang, D.; Xu, T.; Su, L.; Zhang, X.; Dong, H. An open source and reduce expenditure ROS generation strategy for chemodynamic/photodynamic synergistic therapy. *Nat. Commun.* **2020**, *11*, 1735.
(28) Yan, F.; Wu, H.; Liu, H.; Deng, Z.; Liu, H.; Duan, W.; Liu, X.; Zheng, H. Molecular imaging-guided photothermal/photodynamic therapy against tumor by iRGD-modified indocyanine green nanoparticles. *J. Controlled Release* **2016**, *224*, 217−228.
(29) Li, Y.; Lu, W.; Huang, Q.; Li, C.; Chen, W. Copper sulfide nanoparticles for photothermal ablation of tumor cells. *Nanomedicine* **2010**, *5*, 1161−1171.
(30) Shi, H.; Yan, R.; Wu, L.; Sun, Y.; Liu, S.; Zhou, Z.; He, J.; Ye, D. Tumor-Targeting CuS Nanoparticles for Multimodality Imaging and Guided Photothermal Therapy of Lymph Node Metastasis. *Acta Biomater.* **2018**, *72*, 256−265.
(31) Roper, D.; Ahn, W.; Hoepfner, M. Microscale Heat Transfer Transduced by Surface Plasmon Resonant Gold Nanoparticles. *J. Phys. Chem. C Nanomater. Interfaces* **2007**, *111*, 3636−3641.
(32) Friedrich, J.; Seidel, C.; Ebner, R.; Kunz-Schughart, L. Spheroid-based drug screen: considerations and practical approach. *Nat. Protoc.* **2009**, *4*, 309−324.
(33) Yan, F.; Wu, H.; Liu, H.; Deng, Z.; Liu, H.; Duan, W.; Liu, X.; Zheng, H. Molecular imaging-guided photothermal/photodynamic therapy against tumor by iRGD-modified indocyanine green nanoparticles. *J. Controlled Release* **2016**, *224*, 217−228.
(34) Sheng, Z.; Hu, D.; Zheng, M.; Zhao, P.; Liu, H.; Gao, D.; Gong, P.; Gao, G.; Zhang, P.; Ma, Y.; Cai, L. Smart Human Serum Albumin-Indocyanine Green Nanoparticles Generated by Programmed Assembly for Dual-Modal Imaging-Guided Cancer Synergistic Phototherapy. *ACS Nano* **2014**, *8*, 12310−12322.
(35) Aizik, G.; Waiskopf, N.; Agbaria, M.; Ben-David-Naim, M.; Levi-Kalisman, Y.; Shahar, A.; Banin, U.; Golomb, G. Liposomes of Quantum Dots Configured for Passive and Active Delivery to Tumor Tissue. *Nano Lett.* **2019**, *19*, 5844−5852.
(36) Miao, L.; Newby, J.; Lin, C.; Zhang, L.; Xu, F.; Kim, W.; Forest, M.; Lai, S.; Milowsky, M.; Wobker, S.; Huang, L. The Binding Site Barrier Elicited by Tumor-Associated Fibroblasts Interferes Disposition of Nanoparticles in Stroma-Vessel Type Tumors. *ACS Nano* **2016**, *10*, 9243−9258.
(37) Alibolandi, M.; Abnous, K.; Sadeghi, F.; Hosseinkhani, H.; Ramezani, M.; Hadizadeh, F. Folate receptor-targeted multimodal polymersomes for delivery of quantum dots and doxorubicin to breast adenocarcinoma: In vitro and in vivo evaluation. *Int. J. Pharm.* **2016**, *500*, 162−178.
(38) Dai, Y.; Su, J.; Wu, K.; Ma, W.; Wang, B.; Li, M.; Sun, P.; Shen, Q.; Wang, Q.; Fan, Q. Multifunctional Thermosensitive Liposomes Based on Natural Phase Change Material: Near-Infrared Light-Triggered Drug Release and Multimodal Imaging Guided Cancer Combination Therapy. *ACS Appl. Mater. Interfaces* **2019**, *11*, 10540−10553.

https://doi.org/10.1021/acsmaterialslett.2c00707
ACS Materials Lett. 2023, 5, 1−10